Inorg. Chem. **2007**, *46*, 3123–3135

Ditopic N-Crowned 4-(*p*-Aminophenyl)-2,6-diphenylpyridines: Implications of Macrocycle Topology on the Spectroscopic Properties, Cation Complexation, and Differential Anion Responses

Beatriz García-Acosta,[†] Ramón Martínez-Máñez,*[,†] Félix Sancenón,[†] Juan Soto,[†] Knut Rurack,*[,‡] Monika Spieles,[‡] Eduardo García-Breijo,[§] and Luis Gil[§]

Instituto de Química Molecular Aplicada, Departamento de Química, Universidad Politécnica de Valencia, Camino de Vera s/n, E-46071 Valencia, Spain, Division I.5, Bundesanstalt für Materialforschung und -prüfung (BAM), Richard-Willstätter-Strasse 11, D-12489 Berlin, Germany, and Group of Hybrid Microelectronics, Instituto de Investigación en Química Molecular Aplicada, Departamento de Ingeniería Electrónica, Universidad Politécnica de Valencia, Camino Vera s/n, 46071 Valencia, Spain

Received October 30, 2006

A family of N-crowned 4-*p*-(aminophenyl)-2,6-diphenylpyridines **DA** (**1**–**6**) has been synthezised, characterized, and studied as potential hosts for the signaling of cationic and anionic guests. The ditopic probes contain two coordination sites, a monodentate 2,6-diphenylpyridine and an anilino group with macrocycles of different ring size, denticity, and type of secondary heteroatom (O and/or S). X-ray structure analysis of aza–oxa–thia-crowned **5** indicated a largely planar chromophore. Optical spectroscopic and electrochemical studies revealed that the anilino-type donor (**D**) and the 2,6-diphenylpyridine acceptor (**A**) are strongly π-conjugated, entailing intense intramolecular charge-transfer absorption bands at 340 nm. Binding studies with protons and metal ions (**M** = Cu^{2+}, Zn^{2+}, Hg^{2+}, Fe^{3+}, Pb^{2+}, Ni^{2+}, Cd^{2+}) showed shifts of the band to the visible (440 nm) when coordination at the pyridine group occurs, strengthening its acceptor character. In contrast, no band in the visible is formed if binding takes place at the anilino group. Three different responses were found for various pairs of **DA** and **M**: selective metal coordination to **D** or **A** as well as coordination at both sites. A selective response was found for **5** and Hg^{2+}. Because of the multitude of coordination-induced effects, the **DA**–**M** ensembles were further employed for differential anion sensing. In this protocol, the addition of an anion **X** to a certain, weakly coordinated **DA**–**M** can (i) lead to the formation of a ternary ion pair complex (**DA**–**M**–**X**), (ii) change the preference for **A** or **D** coordination, (iii) induce dissociation of the complex, or (iv) can have no effect. Various patterns of absorption changes were obtained as a result of different responses (i)–(iv) of the **DA**–**M**'s in the presence of various **X**'s. Data analysis yielded recognition patterns for acetate, F^- and CN^-, demonstrating the potential of simple chromogenic host–guest pairs for differential anion signaling.

Introduction

The optical response of synthetic host molecules toward cations and anions is of substantial interest in supramolecular and analytical chemistry.[1,2] Metal ion signaling is usually accomplished by chromo- or fluoroionophores that contain a receptor that is either integrated in or covalently attached via a spacer to the chromophore. The coordination event thus modulates the spectroscopic properties of the functional dye molecule, transducing host−guest recognition into a measur-

* To whom correspondence should be addressed. E-mail: rmaez@qim.upv.es (R.M.-M.), knut.rurack@bam.de (K.R.). Phone: 34-963877343 (R.M.-M.), 49-(0)30-8104 5576 (K.R.). Fax: 34-963879349 (R.M.-M.), 49-(0)30-8104 5005 (K.R.).

† Departamento de Química, Universidad Politécnica de Valencia.

‡ Bundesanstalt für Materialforschung and -prüfung.

§ Departamento de Ingeniería Electrónica, Universidad Politécnica de Valencia.

(1) de Silva, A. P.; Gunaratne, H. Q. N.; Gunnlaugsson, T.; Huxley, A. J. M.; McCoy, C. P.; Rademacher, J. T.; Rice, T. E. *Chem. Rev.* **1997**, *97*, 1515−1566. Valeur, B.; Leray, I. *Coord. Chem. Rev.* **2000**, *205*, 3−40. Rurack, K. *Spectrochim. Acta, Part A* **2001**, *57*, 2161−2195. de Silva, A. P.; McCaughan, B.; McKinney, B. O. F.; Querol, M. *Dalton Trans.* **2003**, 1902−1913. Callan, J. F.; de Silva, A. P.; Magri, D. C. *Tetrahedron* **2005**, *61*, 8551−8588.

10.1021/ic062069z CCC: $37.00
Published on Web 03/23/2007

able signal. In the past decade, researchers became increasingly interested in equipping chromophores with more than one chemically addressable group.[3] Such molecules basically integrate various reporter and/or receptor groups that are attached either symmetrically or asymmetrically to suitable dye skeletons such as anthracene, biphenyl, styryl, or other types of dyes.[4,5] These dual-responsive dyes have been mainly designed as so-called "molecular logic gates" and ion-pair indicators but have also been developed for cooperative recognition, i.e., the cooperative recognition of two different analytes as well as the binding of a single analyte with cooperative forces. A closely related strategy[6] developed by Anslyn's group assembles two (or more) different binding sites, one of which is located directly at the chromo- or fluorophore, around a steric control unit, usually a 1,3,5-2,4,6-functionalized, facially segregated benzene.[7] Probably the most serious drawbacks of such approaches are the usually rather time-consuming and complex synthetic procedures involved. Thus, in the latter case, for instance, Anslyn's group emerged to simpler hexasubstituted benzene platforms, incorporating only simple binding groups, while using an external indicator molecule in the fashion of colorimetric displacement assays.[8] The versatility of this approach led to the development of differential receptors[8c] that constitute a set of suitable indicators of slightly varying chemical constitution that respond rather unspecifically yet differently toward a group of related guests.[9] When multicomponent analysis was employed, certain "fingerprint" signal expressions allow researchers to determine single guests via pattern recognition, a concept that was adopted from sophisticated biosensor arrays, electronic noses, and tongues.[10]

Because of our experience in molecular probe design for various analytes[11] and based on our background in bi- and multifunctionalized chromophores,[5a,b,d,e,12] we became interested in developing bifunctional molecular dyes that are facile to synthesize and that can be tuned toward cation- and anion-responsive probes.[13] We envisaged that a suitable combination of the functional subunits of such chemosensors might allow one to follow a different approach toward differential receptors, i.e., the utilization of weak guest−ligand interactions themselves. The basic strategy is outlined in Scheme 1. **D** and **A** are the electron-donating and -accepting units, both in π conjugation, of the auxochromic and fluorescent ligand. They are simple groups such as a receptor-functionalized aniline (**D**) and a 2,6-substituted pyridine (**A**) and, because of the manifoldness of aniline and pyridine chemistry, can thus be principally combined in limitless ways to yield libraries of differential receptors, the step from I to II in Scheme 1. However, when properly designed, a ligand itself can be a selective ionophore for a particular metal ion, as shown in panel III in Scheme 1. On the other hand, if combinations of a ditopic ligand and various metal ions are chosen that show only a moderate affinity for each other at the **A** site, these host−guest pairs (of chromoionophore and metal ion) are assumed to show gradual responses toward a third type of chemical species, e.g., anions. In such a way,

(2) Beer, P. D.; Gale, P. A. *Angew. Chem., Int. Ed.* **2001**, *40*, 486−516. Martínez-Máñez, R.; Sancenón, F. *Chem. Rev.* **2003**, *103*, 4419−4476. Fabbrizzi, L.; Licchelli, M.; Taglietti, A. *Dalton Trans.* **2003**, 3471−3479. Martínez-Máñez, R.; Sancenón, F. *J. Fluoresc.* **2005**, *15*, 267−285. Descalzo, A. B.; Martínez-Máñez, R.; Sancenón, F.; Hoffmann, K.; Rurack, K. *Angew. Chem., Int. Ed.* **2006**, *45*, 5924−5948.

(3) de Silva, A. P.; Fox, D. B.; Moody, T. S.; Weir, S. M. *Trends Biotechnol.* **2001**, *19*, 29−34. de Silva, A. P.; McClenaghan, N. D. *Chem.−Eur. J.* **2004**, *10*, 574−586. de Silva, A. P.; Leydet, Y.; Lincheneau, C.; McClenaghan, N. D. *J. Phys. Condens. Matter* **2006**, *18*, S1847−S1872.

(4) de Silva, A. P.; Gunaratne, H. Q. N.; McCoy, C. P. *J. Am. Chem. Soc.* **1997**, *119*, 7891−7892. Ji, H.-F.; Dabestani, R.; Brown, G. M. *J. Am. Chem. Soc.* **2000**, *122*, 9306−9307. de Silva, S. A.; Amorelli, B.; Isidor, D. C.; Loo, K. C.; Crooker, K. E.; Pena, Y. E. *Chem. Commun.* **2002**, 1360−1361. de Silva, A. P.; McClean, G. D.; Pagliari, S. *Chem. Commun.* **2003**, 2010−2011. Bag, B.; Bharadwaj, P. K. *Chem. Commun.* **2005**, 513−515. Costero, A. M.; Sanchis, J.; Gil, S.; Sanz, V.; Williams, J. A. G. *J. Mater. Chem.* **2005**, *15*, 2848−2853. Kubo, K.; Mori, A. *J. Mater. Chem.* **2005**, *15*, 2902−2907. Lankshear, M. D.; Cowley, A. R.; Beer, P. D. *Chem. Commun.* **2006**, 612−614. Magri, D. C.; Brown, G. J.; McClean, G. D.; de Silva, A. P. *J. Am. Chem. Soc.* **2006**, *128*, 4950−4951. de Sousa, M.; de Castro, B.; Abad, S.; Miranda, M. A.; Pischel, U. *Chem. Commun.* **2006**, 2051−2053.

(5) (a) Rurack, K.; Koval'chuck, A.; Bricks, J. L.; Slominskii, J. L. *J. Am. Chem. Soc.* **2001**, *123*, 6205−6206. (b) Rurack, K.; Bricks, J. L. *Arkivoc* **2001**, 31−40. (c) de Silva, A. P.; McClenaghan, N. D. *Chem.−Eur. J.* **2002**, *8*, 4935−4945. (d) Jiménez, D.; Martínez-Máñez, R.; Sancenón, F.; Ros-Lis, J. V.; Soto, J.; Benito, A.; García-Breijo, E. *Eur. J. Inorg. Chem.* **2005**, 2393−2403. (e) Jiménez, D.; Martínez-Máñez, R.; Sancenón, F.; Soto, J. *Tetrahedron Lett.* **2004**, *45*, 1257−1259.

(6) Hennrich, G.; Anslyn, E. V. *Chem.−Eur. J.* **2002**, *8*, 2218−2224.

(7) Schneider, S. E.; O'Neil, S. N.; Anslyn, E. V. *J. Am. Chem. Soc.* **2000**, *122*, 542−543. Cabell, L. A.; Best, M. D.; Lavigne, J. J.; Schneider, S. E.; Perreault, D. M.; Monahan, M.-K.; Anslyn, E. V. *J. Chem. Soc., Perkin Trans. 2* **2001**, 315−323. Best, M. D.; Anslyn, E. V. *Chem.−Eur. J.* **2003**, *9*, 51−57.

(8) (a) Lavigne, J. J.; Anslyn, E. V. *Angew. Chem., Int. Ed.* **1999**, *38*, 3666−3669. (b) Zhong, Z.; Anslyn, E. V. *J. Am. Chem. Soc.* **2002**, *124*, 9014−9015. (c) Wiskur, S. L.; Floriano, P. N.; Anslyn, E. V.; McDevitt, J. T. *Angew. Chem., Int. Ed.* **2003**, *42*, 2070−2072.

(9) Lavigne, J. J.; Anslyn, E. V. *Angew. Chem., Int. Ed.* **2001**, *40*, 3118−3130.

(10) Nagle, H. T.; Schiffman, S. S.; Gutierrez-Osuna, R. *IEEE Spectrum* **1998**, 22−34. Albert, K. J.; Lewis, N. S.; Schauer, C. L.; Sotzing, G. A.; Stitzel, S. E.; Vaid, T. P.; Walt, D. R. *Chem. Rev.* **2000**, *100*, 2595−2626. Riul, A., Jr.; Malmegrim, R. R.; Fonseca, F. J.; Mattoso, L. H. C. *Artif. Organs* **2003**, *27*, 469−472. Martínez-Máñez, R.; Soto, J.; García-Breijo, E.; Gil, L.; Ibáñez, J.; Llobet, E. *Sens. Actuators, B* **2005**, *104*, 302−307.

(11) (a) Sancenón, F.; Martínez-Máñez, R.; Soto, J. *Chem. Commun.* **2001**, 2262−2263. (b) Rurack, K.; Kollmannsberger, M.; Resch-Genger, U.; Daub, J. *J. Am. Chem. Soc.* **2000**, *122*, 968−969. (c) Sancenon, F.; Martínez-Máñez, R.; Miranda, M. A.; Segui, M.-J.; Soto, J. *Angew. Chem., Int. Ed.* **2003**, *42*, 647−650. (d) Kovalchuk, A.; Bricks, J. L.; Reck, G.; Rurack, K.; Schulz, B.; Szumna, A.; Weisshoff, H. *Chem. Commun.* **2004**, 1946−1947. (e) Ros-Lis, J. V.; García, B.; Jiménez, D.; Martínez-Máñez, R.; Sancenón, F.; Soto, J.; Gonzalvo, F.; Valldecabres, M. C. *J. Am. Chem. Soc.* **2004**, *126*, 4064−4065. (f) Beer, G.; Rurack, K.; Daub, J. *Chem. Commun.* **2001**, 1138−1139. (g) Jiménez, D.; Martínez-Máñez, R.; Sancenón, F.; Ros-Lis, J. V.; Benito, A.; Soto, J. *J. Am. Chem. Soc.* **2003**, *125*, 9000−9001. (h) Sancenón, F.; Descalzo, A. B.; Martínez-Máñez, R.; Miranda, M. A.; Soto, J. *Angew. Chem., Int. Ed.* **2001**, *40*, 2640−2643. (i) Ros-Lis, J. V.; Martínez-Máñez, R.; Benito, A.; Soto, J. *Polyhedron* **2006**, *25*, 1585−1591. (j) Ros-Lis, J, V.; Martínez-Máñez, R.; Soto, J. *Chem. Commun.* **2005**, 5260−5262. (k) Casasús, R.; Aznar, E.; Marcos, M. D.; Martínez-Máñez, R.; Sancenón, F.; Soto, J.; Amorós, P. *Angew. Chem., Int. Ed.* **2006**, *45*, 6661.

(12) (a) Sancenón, F.; Benito, A.; Hernández, F. J.; Lloris, J. M.; Martínez-Mánez, R.; Pardo, T.; Soto, J. *Eur. J. Inorg. Chem.* **2002**, 866−875. (b) Unger, B.; Rurack, K.; Müller, R.; Jancke, H.; Resch-Genger, U. *J. Mater. Chem.* **2005**, *15*, 3069−3083.

(13) (a) Descalzo, A. B.; Martínez-Máñez, R.; Radeglia, R.; Rurack, K.; Soto, J. *J. Am. Chem. Soc.* **2003**, *125*, 3418−3419. (b) Descalzo, A. B.; Rurack, K.; Weisshoff, H.; Martínez-Máñez, R.; Marcos, M. D.; Amorós, P.; Hoffmann, K.; Soto, J. *J. Am. Chem. Soc.* **2005**, *127*, 184−200.

Scheme 1 [a]

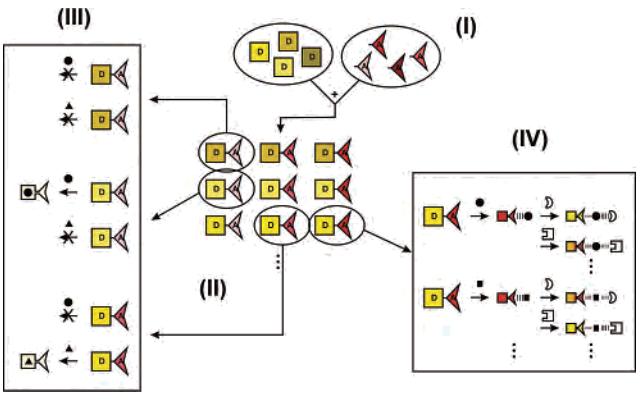

[a] (I) Pool of donor building blocks (**D**, greenish-yellow squares), functionalized with specific receptors, and acceptor building blocks (**A**, reddish-pink triangles), carrying nonspecific binding sites. The deepness of the color indicates the donor or acceptor strength. (II) Library of chromophoric CT-active ligands **DA** obtained by coupling **D** and **A** units. (III) Selectivity pattern toward various metal ions (black symbols). Only selected cations bind to **D**, inducing a decrease in CT character as indicated by the pale yellow color. (IV) Unselective binding of various metal ions (black symbols) to the **A** unit, inducing an increase in CT character as indicated by the strong red color. These complexes show a differential response toward various anions (white symbols) through ion pairing, with the strength of the latter process determining the degree of CT weakening as sketched by the different colors.

a potentially highly selective molecular system can be transformed into an ensemble that can be employed for unspecific but differential recognition; see panel IV in Scheme 1.

After having recently shown the proof-of-principle of the creation of a differential sensing array for anions based on weak metal−ligand interactions,[14] we report here a comprehensive study of the synthesis and molecular properties of a series of differently crowned anilinopyridines (i.e., we kept **A** in Scheme 1 constant while varying **D**) and their coordination features toward metal ions and address issues of the anion-signaling behavior of the coordinative metal−ligand ensembles.

Experimental Section

Materials. All commercially available reagents were used without further purification. Air/water-sensitive reactions were performed in flame-dried glassware under argon. Acetonitrile (ACN) was dried with CaH_2 and distilled prior to use. The additional solvents employed for the photophysical studies, *n*-hexane (HEX), di-*n*-butyl ether, diethyl ether (EOE), tetrahydrofuran, acetone (ACE), and propionitrile, were of UV-spectroscopic grade and were purchased from Fluka, Merck, and Aldrich. Perchlorate salts of Pb^{2+}, Fe^{3+}, Ni^{2+}, and Cd^{2+} and triflate salts of Hg^{2+} and Zn^{2+} were purchased from Aldrich, whereas the triflate salt of Cu^{2+} was purchased from Acros. The anions were used as tetrabutylammonium salts and were purchased from Aldrich (Cl^-, Br^-, I^-, NO_3^-, AcO^-, SCN^-, and CN^-) and Fluka (F^-). Tetra-*n*-butylammonium perchlorate (Fluka) for the electrochemical experiments was recrystallized and dried under vacuum for at least 48 h.

Synthesis. General Procedure for 1−6. The Richman−Atkins procedure[15] was used to synthesize the crowned anilino precursors **II**−**VI**,[5d,16] which were then dissolved in dry *N*,*N*-dimethylformamide and reacted with 2 equiv of 2,6-diphenylpyrylium perchlorate (**VII**) for 3 h at 150 °C; in the same way, *N*,*N*-dimethylaniline (**I**) was used for **1**. After cooling to room temperature, EOE was added and a magenta-colored oil was separated. The oil was decanted and dissolved in ACE, and aqueous ammonium hydroxide was added (15% v/v, 2 mL) until the magenta color of the solution changed to brown-yellowish. The crude residue was concentrated on a rotary evaporator and purified by column chromatography on aluminum oxide with mixtures of dichloromethane−ethyl acetate [1:1 (v/v)] as the eluent. The final receptors were obtained as yellowish solids.

4-(2,6-Diphenylpyridin-4-yl)-*N*,*N*-dimethylaniline (1). A total of 3.95 mmol of **I** and 7.9 mmol of **VII**[17] resulted in 1.57 mmol of **1**. Yield: 40%. ^{1}H NMR (300 MHz, $CDCl_3$): δ 3.05 (s, 6H, CH_3), 6.87 (d, 2H, J = 8 Hz, C_6H_4), 7.54 (t, 3H, J = 7.5 Hz, C_6H_5), 7.63 (t, 3H, J = 7.5 Hz, C_6H_5), 7.75 (d, 2H, J = 8 Hz, C_6H_4), 7.96 (s, 2H, C_5H_2N), 8.34 (d, 4H, J = 8 Hz, C_6H_5). ^{13}C NMR (75 MHz, $CDCl_3$): δ 40.33 (CH_3), 112.45 (C_6H_4), 115.96 (C_5H_2N), 127.09, 127.78 (C_6H_4), 128.59, 128.77, 139.89 (C_6H_5), 149.74 (C_6H_4), 151.01, 157.23 (C_5H_2N). MS (FAB$^+$): *m*/*z* 350 (M^+). Elem anal. Calcd for $C_{25}H_{22}N_2$: C, 85.68; H, 6.33; N, 8.00. Found: C, 85.75; H, 6.44; N, 7.92.

10-[4-(2,6-Diphenylpyridin-4-yl)phenyl]-1,4,7-trioxa-10-azacyclododecane (2). A total of 1.39 mmol of **II**[5d] and 2.78 mmol of **VII**[17] resulted in 0.51 mmol of **2**. Yield: 37%. ^{1}H NMR (300 MHz, $CDCl_3$): δ 3.62 (m, 12H, CH_2), 3.90 (t, 4H, J = 7 Hz, CH_2), 6.84 (d, 2H, J = 8 Hz, C_6H_4), 7.41 (t, 3H, J = 7.5 Hz, C_6H_5), 7.47 (t, 3H, J = 7.5 Hz, C_6H_5), 7.63 (d, 2H, J = 8 Hz, C_6H_4), 7.72 (s, 2H, C_5H_2N), 8.16 (d, 4H, J = 8 Hz, C_6H_5). ^{13}C NMR (75 MHz, $CDCl_3$): δ 53.14, 70.11, 70.48, 72.15 (CH_2), 113.21 (C_6H_4), 116.46 (C_5H_2N), 127.67, 128.39 (C_6H_4), 129.18, 129.35, 140.59 (C_6H_5), 149.94 (C_6H_4), 150.35, 157.86 (C_5H_2N). MS (FAB$^+$): *m*/*z* 480 (M^+). Elem anal. Calcd for $C_{31}H_{32}N_2O_3$: C, 77.47; H, 6.71; N, 5.83. Found: C, 77.50; H, 6.75; N, 5.78.

13-[4-(2,6-Diphenylpyridin-4-yl)phenyl]-1,4,7,10-tetraoxa-13-azacyclopentadecane (3). A total of 1.15 mmol of **III**[16] and 2.30 mmol of **VII**[17] resulted in 0.49 mmol of **3**. Yield: 43%. ^{1}H NMR (300 MHz, $CDCl_3$): δ 3.65 (m, 16H, CH_2), 3.72 (t, 4H, J = 7 Hz, CH_2), 6.80 (d, 2H, J = 8 Hz, C_6H_4), 7.44 (t, 3H, J = 7.5 Hz, C_6H_5), 7.52 (t, 3H, J = 7.5 Hz, C_6H_5), 7.67 (d, 2H, J = 8 Hz, C_6H_4), 7.86 (s, 2H, C_5H_2N), 8.20 (d, 4H, J = 8 Hz, C_6H_5). ^{13}C NMR (75 MHz, $CDCl_3$): δ 52.56, 68.39, 70.07, 70.20, 71.28 (CH_2), 111.75 (C_6H_4), 115.83 (C_5H_2N), 127.06, 127.95 (C_6H_4), 128.56, 128.73, 139.94 (C_6H_5), 148.32 (C_6H_4), 149.72, 157.24 (C_5H_2N). MS (FAB$^+$): *m*/*z* 524 (M^+). Elem anal. Calcd for $C_{33}H_{36}N_2O_4$: C, 75.55; H, 6.92; N, 5.34. Found: C, 75.60; H, 6.95; N, 5.30.

16-[4-(2,6-Diphenylpyridin-4-yl)phenyl]-1,4,7,10,13-pentaoxa-16-azacyclooctadecane (4). A total of 1.86 mmol of **IV**[16] and 3.72 mmol of **VII**[17] resulted in 0.78 mmol of **4**. Yield: 42%. ^{1}H NMR (300 MHz, $CDCl_3$): δ 3.65 (m, 20H, CH_2), 3.70 (t, 4H, J = 7 Hz, CH_2), 6.80 (d, 2H, J = 8 Hz, C_6H_4), 7.45 (t, 3H, J = 7.5 Hz, C_6H_5), 7.51 (t, 3H, J = 7.5 Hz, C_6H_5), 7.65 (d, 2H, J = 8 Hz, C_6H_4), 7.85 (s, 2H, C_5H_2N), 8.20 (d, 4H, J = 8 Hz, C_6H_5). ^{13}C NMR (75 MHz, $CDCl_3$): δ 51.04, 68.50, 70.60, 70.67 (CH_2), 111.76 (C_6H_4), 115.72 (C_5H_2N), 125.44 (C_6H_5), 126.99, 127.89 (C_6H_4), 128.50, 128.68,

(14) García-Acosta, B.; Albiach-Martí, X.; García, E.; Gil, L.; Martínez-Máñez, R.; Rurack, K.; Sancenón, F.; Soto, J. *Chem. Commun.* **2004**, 774−775.

(15) Richman, J. E.; Atkins, T. J. *J. Am. Chem. Soc.* **1974**, *96*, 2268−2270. Atkins, T. J.; Richman, J. E.; Oettle, W. F. *Org. Synth.* **1978**, *58*, 86−98. Krakowiak, K. E.; Bradsahw, J. S.; Zamecka-Krakowiak, D. J. *Chem. Rev.* **1989**, *89*, 929−972.

(16) Dix, J. P.; Vögtle, F. *Angew. Chem., Int. Ed. Engl.* **1978**, *17*, 857−859.

(17) Doddi, G.; Ercolani, G. *Synthesis* **1985**, 789−790. Pikus, A. L.; Feigelman, V. M.; Mezheritskii, V. V. *Zhur. Org. Khim.* **1989**, *25*, 2603−2608.

139.85 (C_6H_5), 148.56 (C_6H_4), 149.63, 157.17 (C_5H_2N). MS (FAB^+): *m/z* 568 (M^+). Elem anal. Calcd for $C_{35}H_{40}N_2O_5$: C, 73.92; H, 7.09; N, 4.93. Found: C, 73.98; H, 7.05; N, 4.98.

10-[4-(2,6-Diphenylpyridin-4-yl)phenyl]-1,4-dioxa-7,13-dithia-10-azacyclopentadecane (5). A total of 2.45 mmol of **V**[5d] and 4.90 mmol of **VII**[17] resulted in 1.10 mmol of **5**. Yield: 45%. ^{1}H NMR (300 MHz, $CDCl_3$): δ 2.77 (t, 4H, J = 6.5 Hz, CH_2), 2.94 (t, 4H, J = 7 Hz, CH_2), 3.62 (s, 2H, CH_2), 3.70 (t, 4H, J = 7 Hz, CH_2), 3.82 (t, 4H, J = 6.5 Hz, CH_2), 6.76 (d, 2H, J = 8 Hz, C_6H_4), 7.41 (t, 3H, J = 7.5 Hz, C_6H_5), 7.50 (t, 3H, J = 7.5 Hz, C_6H_5), 7.67 (d, 2H, J = 8 Hz, C_6H_4), 7.82 (s, 2H, C_5H_2N), 8.18 (d, 4H, J = 8 Hz, C_6H_5). ^{13}C NMR (75 MHz, $CDCl_3$): δ 29.47, 31.24, 51.88, 70.73, 74.37 (CH_2), 112.04 (C_6H_4), 115.92 (C_5H_2N), 126.00 (C_6H_5), 127.10, 128.20 (C_6H_4), 128.61, 128.78, 139.95 (C_6H_5), 147.59 (C_6H_4), 149.66, 157.30 (C_5H_2N). MS (FAB^+): *m/z* 556 (M^+). Elem anal. Calcd for $C_{33}H_{36}N_2O_2S_2$: C, 71.19; H, 6.52; N, 5.03. Found: C, 71.03; H, 6.48; N, 4.98.

13-[4-(2,6-Diphenylpyridin-4-yl)phenyl]-1,10-dioxa-4,7-dithia-13-azacyclopentadecane (6). A total of 1.84 mmol of **VI**[5d] and 3.68 mmol of **VII**[17] resulted in 0.745 mmol of **6**. Yield: 40.5%. ^{1}H NMR (300 MHz, $CDCl_3$): δ 2.74 (t, 4H, J = 7 Hz, CH_2), 2.90 (s, 4H, CH_2), 3.62−3.80 (m, 12H, CH_2), 6.80 (d, 2H, J = 8 Hz, C_6H_4), 7.45 (t, 3H, J = 7.5 Hz, C_6H_5), 7.52 (t, 3H, J = 7.5 Hz, C_6H_5), 7.67 (d, 2H, J = 8 Hz, C_6H_4), 7.84 (s, 2H, C_5H_2N), 8.19 (d, 4H, J = 8 Hz, C_6H_5). ^{13}C NMR (75 MHz, $CDCl_3$): δ 31.66, 32.84, 51.22, 69.67, 72.14 (CH_2), 112.25 (C_6H_4), 115.92 (C_5H_2N), 126.22 (C_6H_5), 127.10, 128.02 (C_6H_4), 128.61, 128.81, 139.91 (C_6H_5), 149.02 (C_6H_4), 149.62, 157.33 (C_5H_2N). MS (FAB^+): *m/z* 556 (M^+). Elem anal. Calcd for $C_{33}H_{36}N_2O_2S_2$: C, 71.19; H, 6.52; N, 5.03. Found: C, 70.88; H, 6.56; N, 5.00.

Structure determination of 5: $C_{33}H_{36}N_2O_2S_2$, M = 556.76, monoclinic space group $P2_1/n$, a = 8.548(2) Å, b = 10.067(2) Å, c = 33.777(8) Å, β = 90.10(2)°, Z = 4, V = 2906.7(10) Å^3, D_{calcd} = 1.272 g cm^{-3}, λ(Mo Kα) = 0.710 73 Å, T = 293(2) K, μ(Mo Kα) = 0.216 mm^{-1}. Measurements were carried out using a Siemens P4 diffractometer with graphite-monochromated Mo Kα radiation on a single crystal of dimensions 0.26 × 0.25 × 0.10 mm. A total of 6864 reflections were collected, of which 5069 were independent (R_{int} = 0.0284). Lorentz, polarization, and absorption (ψ scan, max and min transmission 0.838 and 0.898) corrections were applied. The structure was solved by direct methods (*SHELXTL*)[18] and refined by full-matrix least-squares analysis on F^2 (*SHELXTL*). The refinement converged at R1 = 0.0429 [$F > 4\sigma(F)$] and wR2 = 0.2270 (all data). Largest peak and hole in the final difference map +0.224 and −0.233 e Å^3. CCDC-286788 contains the supplementary crystallographic data for this paper. These data can be obtained free of charge from The Cambridge Crystallographic Data Centre via www.cam.ac.uk/data_request/cif.

Optical Spectroscopy. UV/vis spectra were recorded on Bruins Instruments Omega 10 and Perkin-Elmer Lambda 35 spectrophotometers, steady-state fluorescence spectra on a Spectronics Instruments 8100 fluorometer (90° standard geometry, polarizers at 0° and 54.7° in excitation and emission), and an Edinburgh Analytical Instruments FS900CDT fluorometer. All photophysical measurements were carried out at 298 ± 1 K with dilute solutions with optical densities between 0.03 and 0.05 at the absorption maximum for HEX solutions and between 0.08 and 0.1 for the other solvents. Molar absorbances were determined from N = 8 samples. Fluorescence quantum yields (Φ_f) were determined relative to quinine sulfate dihydrate (NIST standard reference material SRM 936) in 0.1 N H_2SO_4 (Φ_f = 0.51 ± 0.03)[19] for the species with absorption maxima in the 320−340 nm region and relative to coumarin 153 in ethanol (Φ_f = 0.40)[20] for the species with absorption maxima in the 430−440 nm region with uncertainties of ±3% (for $\Phi_f > 0.2$), ±6% (for $0.2 > \Phi_f > 0.02$), ±10% (for $0.02 > \Phi_f > 5 \times 10^{-3}$), and ±15% (for $5 \times 10^{-3} > \Phi_f$), respectively. All of the fluorescence spectra were corrected as described in ref 21. The Stokes shifts were calculated from the differences between the maxima of the absorption and emission bands after conversion to the energy scale, taking into account another correction step.[22] **1**−**6** were used in ca. 5.0 × 10^{-5} and ca. 3.0 × 10^{-5} M for the spectrophotometric and fluorometric complexation experiments, respectively. Cations and anions were used in equimolar quantities.

Fluorescence lifetimes (τ_f) were measured with a unique laser impulse fluorometer with picosecond time resolution described by us in an earlier publication[23] and modified according to a description in ref 24. The fourth-harmonic output of the signal of the optical parametric amplifier was used for excitation, the fluorescence was collected at right angles (polarizer at 54.7°; monochromator with bandwidths of 4, 8, and 16 nm), and the decays were recorded by the single-photon timing method (typical instrumental response functions of 25−30 ps full width at half-maximum; experimental accuracy of ±3 ps). The laser beam was attenuated using a double-prism attenuator from LTB, and typical excitation energies were in the nanowatt to microwatt range (average laser power). The fluorescence lifetime profiles were analyzed with a PC using the software package Global Unlimited V2.2 (Laboratory for Fluorescence Dynamics, University of Illinois, Urbana-Champaign, IL). The goodness of the fit of the single decays as judged by reduced χ^2 (χ_R^2) and the autocorrelation function $C(j)$ of the residuals was always below $\chi_R^2 < 1.2$.

Measurements of the pH. For every step of the pH titration, small amounts of 11.2 M (70% by weight) $HClO_4$ were added (microliter pipet; Eppendorf) to 50 mL of a solution containing 90 μM dye in an ethanol−water mixture [1:1 (v/v)]. After stirring for 3 min, 3 mL of the solution was transferred to a 10 mm quartz cuvette and additionally stirred for 1 min. The pH was monitored using a digital pH meter (WTW pH 537) equipped with a glass electrode (Mettler Toledo InLab 423). Calibration of the instrument was performed with standard aqueous solutions of pH = 1.68, 4.01, 6.86, and 9.18 from WTW. The measured value (pH^{mes}) was corrected by taking into account differences in the liquid junction potentials (ΔU_j) and proton activity coefficients ($\Delta \log \gamma_{H+}$) between the solvent mixture of the sample and the aqueous calibration solution according to eq 1.[25]

$$pH = pH^{mes} - \Delta U_j + \Delta \log \gamma_{H^+} = pH^{mes} - 0.21 \qquad (1)$$

From multiple titrations (N = 4), the error of pH^{mes} in the range of $1 < pH < 6$ was determined to be ±0.2 pH units. The pH values of the highly acidic samples were directly calculated from the

(18) *SHELXTL*, version 5.03; Siemens Analytical X-ray Instruments: Madison, WI, 1994.

(19) Velapoldi, R. A. In *Advances in Standards and Methodology in Spectorphotometry*; Burgess, C., Mielenz, K. D., Eds.; Elsevier Science: Amsterdam, The Netherlands, 1987; pp 175−193.
(20) Drexhage, K.-H. *J. Res. Natl. Bur. Stand.* **1976**, *80A*, 421−428.
(21) Resch-Genger, U.; Pfeifer, D.; Monte, C.; Pilz, W.; Hoffmann, A.; Spieles, M.; Rurack, K.; Hollandt, J.; Taubert, D.; Schönenberger, B.; Nording, P. *J. Fluoresc.* **2005**, *15*, 315−336.
(22) Lakowicz, J. R. *Principles of Fluorescence Spectroscopy*, 2nd ed.; Plenum: New York, 1999; p 52.
(23) Resch, U.; Rurack, K. *Proc. SPIE−Int. Soc. Opt. Eng.* **1997**, *3105*, 96−103.
(24) Shen, Z.; Röhr, H.; Rurack, K.; Uno, H.; Spieles, M.; Schulz, B.; Reck, G.; Ono, N. *Chem.−Eur. J.* **2004**, *10*, 4853−4871.
(25) Galster, H. *pH Measurement*; Wiley-VCH: Weinheim, Germany, 1991.

Scheme 2. Reaction Scheme for the Synthesis of **1**−**6** from **I**−**VI** Precursors

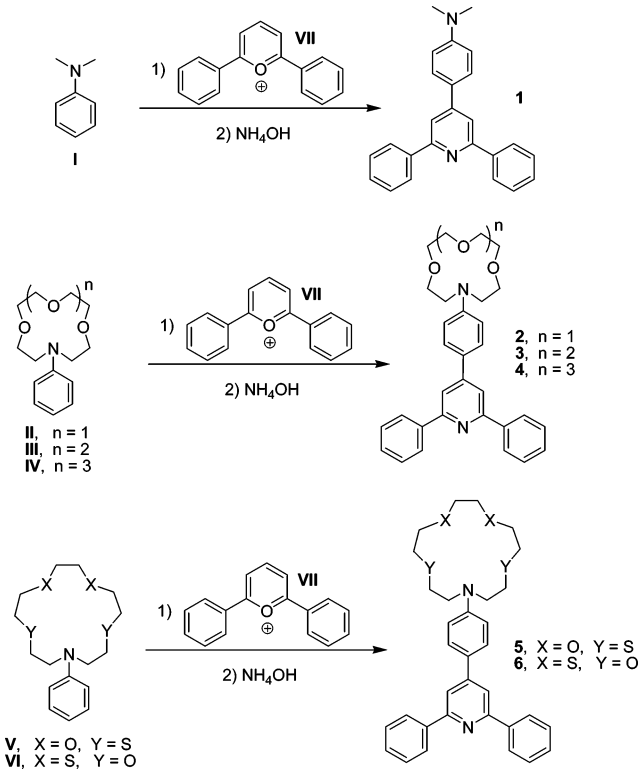

analytical acid concentrations in the respective solvent mixtures without correction for the activity coefficient ($\gamma_{\pm}$).

NMR Spectroscopy. ^{1}H NMR studies in the presence of selected cations were carried out with a Varian Gemini spectrometer by titrating 1 mM solutions of the receptor with 0.1−5 equiv of the corresponding cation.

Electrochemistry. Cyclic voltammetry, rotating-disk electrode, and differential pulse voltammetry experiments were carried out in dry and degassed ACN with a programmable function generator Tacussel IMT-1, connected to a Tacussel PJT 120-1 potentiostat, with a Pt working electrode, a saturated calomel electrode (SCE) reference electrode, a Pt wire auxiliary electrode, and a 0.1 M $[Bu_4N][ClO_4]$ supporting electrolyte. Rotating-disk electrode experiments were run at a scan speed of 10 mV s^{-1} and a rotation speed of 7000 revolutions min^{-1} on 1 mM solutions of the dyes. Differential pulse voltammetry was carried out with a pulse amplitude of 10 mV, a sweep rate of 2 mV s^{-1}, and a "drop time" of 0.5 s.

Results and Discussion

Ligands **2**−**6** are a group of 4-(N-crown)phenyl-2,6-diphenylpyridines that carry different monoaza macrocycles as crown substituents, varying both in ring size and the number and type of secondary heteroatoms (O and/or S; Scheme 2). The *N*,*N*-dimethylamino analogue **1** was studied as a model compound. To get an idea of the molecular geometry and the degree of π conjugation in the chromophore as well as the integration of the receptor's N atom into the π system, the crystal structure of **5** was determined exemplarily. The manifestation of both aspects, π conjugation as a function of the planarity in the chromophore and decoupling of the N atom as a function of pyramidalization, in an X-ray structure has been shown by others and us to provide valuable information on the putative conformation in solution and photophysical mechanisms.[11d,12a,24,26] Suitable crystals for X-ray diffraction were obtained by slow diffusion of HEX into dichloromethane solutions of **5**. Table 1 lists selected bond lengths and angles, and Figure 1 shows a view of the compound with the numbering scheme. In the macrocyclic ring of **5**, average C−S, C−O, C−N, and C−C distances are 1.795(3), 1.412(3), 1.457(3), and 1.502(4) Å, respectively. The twist angle between the planes defined by the rings C(1)−C(2)−C(3)−C(4)−C(5)−C(6) and C(7)−C(8)−C(9)−N(2)−C(22)−C(23) is 21.5°, whereas the twist angles between the pyridine ring and the rings C(16)−

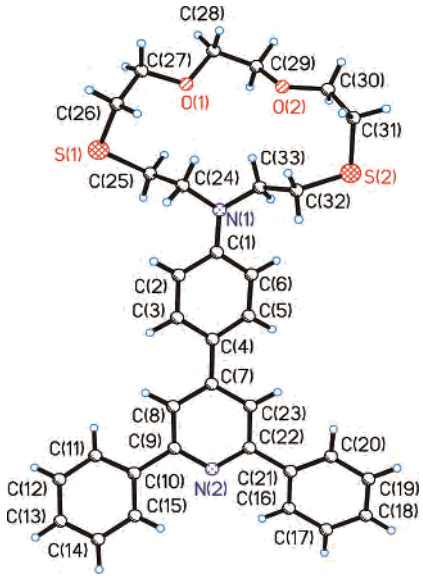

Figure 1. Molecular structure of **5** showing the atom numbering scheme.

Table 1. Selected Distances and Bond Angles for Compound **5**

Distances (Å)			
S(1)−C(26)	1.796(3)	S(1)−C(25)	1.805(3)
S(2)−C(31)	1.786(3)	S(2)−C(32)	1.805(3)
N(1)−C(1)	1.459(3)	N(1)-C(33)	1.454(3)
N(1)−C(24)	1.459(3)	O(1)−C(27)	1.424(3)
O(2)−C(30)	1.415(3)	C(28)−C(29)	1.489(4)
C(26)−C(27)	1.494(4)	C(32)−C(33)	1.513(3)
C(4)−C(7)	1.475(3)	N(2)−C(9)	1.349(3)
N(2)−C(22)	1.341(3)	C(22)−C(23)	1.388(3)
C(11)−C(12)	1.380(4)	C(9)−C(10)	1.488(3)
Angles (deg)			
C(26)−S(1)−C(25)	103.43(12)	C(31)−S(2)−C(32)	104.14(14)
C(1)−N(1)−C(33)	121.4(2)	C(1)−N(1)−C(24)	121.2(2)
C(33)−N(1)−C(24)	117.4(2)	C(22)−N(2)−C(9)	117.8(2)
C(28)−O(1)−C(27)	112.7(2)	N(1)−C(1)−C(2)	122.3(2)
N(1)−C(1)−C(6)	121.2(2)	C(2)−C(19)−C(6)	116.4(4)
C(5)−C(4)−C(7)	121.7(2)	C(8)−C(27)−C(23)	116.1(2)
N(2)−C(9)−C(8)	122.3(2)	C(8)−C(9)−C(10)	122.4(2)
C(11)−C(10)−C(9)	122.0(2)	C(16)−C(21)−C(22)	120.3(2)
N(2)−C(22)−C(21)	116.5(2)	N(1)−C(33)−C(32)	111.8(2)
C(24)−C(25)−S(1)	113.8(2)	C(27)−C(26)−S(1)	117.1(2)
O(2)−C(29)−C(28)	111.0(3)	O(2)−C(30)−C(31)	110.3(3)
C(30)−C(31)−S(2)	117.2(2)	C(33)−C(32)−S(2)	114.6(2)

(26) (a) Jonker, S. A.; van Dijk, S. I.; Goubitz, K.; Reiss, C. A.; Schuddeboom, W.; Verhoeven, J. W. *Mol. Cryst. Liq. Cryst.* **1990**, *183*, 273−282. (b) Jonker, S. A.; Verhoeven, J. W.; Reiss, C. A.; Goubitz, K.; Heijdenrijk, D. *Recl. Trav. Chim. Pays-Bas* **1990**, *109*, 154−159. (c) Rurack, K.; Bricks, J. L.; Reck, G.; Radeglia, R.; Resch-Genger, U. *J. Phys. Chem. A* **2000**, *104*, 3087−3109. (d) Rurack, K.; Bricks, J. L.; Schulz, B.; Maus, M.; Reck, G.; Resch-Genger, U. *J. Phys. Chem. A* **2000**, *104*, 6171−6188.

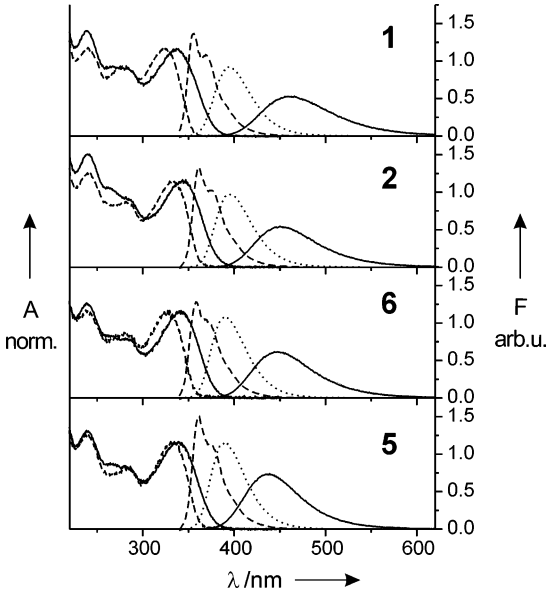

Figure 2. Normalized absorption and relative emission spectra of **1**, **2**, **5**, and **6** in HEX (dashed line), EOE (dotted line), and ACN (solid line) at room temperature. The absorption spectra in EOE were omitted for clarity.

C(17)−C(18)−C(19)−C(20)−C(21) and C(10)−C(11)−C(12)−C(13)−C(14)−C(15) are 18.2° and 23.4°, respectively. The former intramolecular twist angle that is important for the degree of conjugation in the main chromophore is comparable to related 4-phenylpyridines,[27] suggesting that the molecules should possess intense charge-transfer (CT) absorption bands.

Optical Spectroscopy of 1, 2, 5, and 6. A key step in the development of optically responsive host molecules is the understanding of their electronic properties with regard to the desired signaling reaction. Topology in terms of the arrangement and nature of the donor atoms in a crown ether binding unit determines the selectivity of such a host, yet these two factors also influence the ionization potential of the bridgehead atom that connects the π system and receptor and the flexibility of the receptor unit and thus feedback on the photophysical properties. Changes in the ionization potential are reflected by shifts in the spectral band position and redox potential; the flexibility can affect the fluorescence yield of such molecules. The spectroscopic behavior of four of the dyes was thus exemplarily studied in a series of solvents and correlated with the electrochemical data obtained in ACN.

Figure 2 shows representative absorption and emission spectra of the four compounds in solvents of different polarity. The corresponding data are collected in Table 2. The lowest-energy absorption bands are broad and structureless for all combinations of dye and solvent and centered at ca. 330 nm in HEX and ca. 340 nm in ACN. In contrast to these minor shifts, the emission bands are strongly red-shifted from ca. 360 to 450 nm and broadened with increasing solvent polarity. The Stokes shifts increase from ca. 2500 cm^{-1} in nonpolar HEX to ≥7200 cm^{-1} in highly polar ACN (Table 2). Molar absorptivities lie between 24 000 and 30 000 M^{-1} cm^{-1}, and the overall integrals of the lowest-energy absorption bands, i.e., the oscillator strengths, are very similar for each dye in the series of solvents. The fluorescence quantum yields Φ_f of all of the molecules amount to ca. 0.50 ± 0.10 irrespective of the solvent considered, qualifying the compounds as highly emissive fluorophores. Despite this similarity in Φ_f, the fluorescence lifetimes τ_f show an apparent trend for all four compounds and increase from ca. 1.1 to 3.3 ns upon going from a nonpolar to a highly polar solvent. However, all of the fluorescence decay profiles are strictly monoexponential. This apparent contradiction of constant Φ_f but changing τ_f, which would indicate a change in the radiative rate constant $k_r = \Phi_f/\tau_f$ (e.g., 4.4 × 10^8 s^{-1} vs 1.5 × 10^8 s^{-1} for **2** in HEX vs ACN) and thus a change of the nature of the emitting state as a function of the solvent polarity, does not hold if the dependence of the rate constant on the emission energy is taken into account by comparing the reduced rate constants κ_f (Table 3).[28] Thus, the high Φ_f values and single-exponential decays in combination with broad, structureless, and intense absorption bands over the entire solvent spectrum suggest that allowed ICT transitions are responsible for $S_1 \leftarrow S_0$ absorption as well as for the radiative deactivation of the first excited singlet state of thetitle dyes. These findings are supported by a solvatochromic analysis of the data, where linear plots of the Stokes shifts versus a solvent polarity function yield acceptable

Table 2. Spectroscopic Properties and Nonradiative Rate Constants k_{nr} of **1**, **2**, **5**, and **6** in Three Representative Solvents of Different Polarity at 298 K (for Corresponding Spectra, See Figure 2)

	solvent[a]	λ_{abs}/nm	λ_{em}/nm	$\tilde{\nu}_{abs-em}$[b]/cm^{-1}	Φ_f	τ_f/ns	$k_{nr}/10^8$ s^{-1}
1	ACN	336	461	8490	0.52	3.73	1.3
	EOE	329	395	5250	0.47	1.59	3.3
	HEX	324	359	2770	0.49	1.21	4.2
2	ACN	343	451	7330	0.48	3.29	1.6
	EOE	337	396	4550	0.50	1.61	3.1
	HEX	333	365	2370	0.49	1.12	4.5
5	ACN	338	437	7030	0.58	2.86	1.5
	EOE	335	390	4390	0.56	1.43	3.1
	HEX	333	364	2370	0.54	1.07	4.3
6	ACN	341	447	7330	0.53	3.22	1.5
	EOE	333	391	4610	0.53	1.46	3.2
	HEX	327	362	2670	0.48	1.12	4.6

[a] For abbreviations, see the Experimental Section. [b] Obtained as described in the Experimental Section.

Table 3. Average Reduced Rate Constants κ_f and Results[a] of the Solvatochromic Analysis [$\tilde{\nu}_{abs-em}$ vs $f(\epsilon) - f(n^2)$; Linear Fit][29] for **1**, **2**, **5**, and **6** in the Solvents Listed in the Experimental Section

	κ_f[b]/10^{-7} s^{-1} cm^3	slope[a]/cm^{-1}	intercept[a]/cm^{-1}	r^a
1	75 ± 17	18 300 ± 1000	2570 ± 210	0.993
2	78 ± 15	15 400 ± 1000	2230 ± 200	0.991
5	91 ± 17	14 500 ± 1100	2240 ± 220	0.990
6	82 ± 15	14 500 ± 900	2490 ± 200	0.991

[a] The κ_f data for each compound within a series of solvents do not show significant trends. [b] The κ_f data for each compound within a series of solvents do not show significant trends.

(27) Van Eerden, J.; Grootenhuis, P. D. J.; Dijkstra, P. J.; Van Staveren, P. J.; Harkema, S.; Reinhoudt, D. N. *J. Org. Chem.* **1986**, *51*, 3918−3920. Ondracek, J.; Novotny, J.; Petru, M.; Lhotak, P.; Kuthan, J. *Acta Crystallogr.* **1994**, *C50*, 1809−1811. Anulewicz, R.; Bak, T.; Cyranski, M.; Krygowski, T. M.; Rasala, D.; Swirska, B. *Pol. J. Chem.* **1995**, *69*, 597−604.

(28) $\kappa_f = k_f/\langle n^3\tilde{\nu}_{em}{}^3\rangle$ with $\langle n^3\tilde{\nu}_{em}{}^3\rangle \approx n^3(\sum\tilde{\nu}_{em}{}^3/I_{\tilde{\nu}_{em}}\sum I_{\tilde{\nu}_{em}})$, $k_f = \Phi_f/\tau_f$, n = refractive index of the solvent, $\tilde{\nu}_{em}$ = emission wavenumber, and $I_{\tilde{\nu}_{em}}$ = emission intensity at $\tilde{\nu}_{em}$. See: Birks, J. B. *Photophysics of Aromatic Molecules*; Wiley-Interscience: London, 1970.

correlations with $r > 0.99$ in all of the four cases (Table 3).[29] If we assume that the conformation of the dyes in the ground state in solution is close to that found in the X-ray structural analysis (probably including packing effects in the crystal) and that obtained by quantum chemical geometry optimizations at the semiempirical level for the isolated molecules, then the interannular twist angle should amount to $\theta \sim 30°$.[30] In agreement with recent findings on donor−acceptor-substituted biphenyls,[31] a vibrational analysis of the fluorescence bands in HEX yielding the highest relative intensity for the 0−0 band with respect to the second vibronic band (e.g., ratios of 1:0.84 and 1:0.78 for **1** and **5**) suggests that the emitting state of the anilinopyridines also possesses a more planar conformation and an angular distribution of $\theta \sim 0°$.[32] The $S_1 \leftarrow S_0$ transition and the (relaxed) Franck−Condon excited state thus have a considerable CT character. The Franck−Condon state then populates the emissive state on the subpicosecond time scale, the latter of which has a more planar conformation and a higher dipole moment, i.e., a more pronounced ICT character. The respective change in the dipole moment ($\mu_e - \mu_g$) is calculated to 18.2 D for **1**, 16.7 D for **2**, and 16.2 D for both **5** and **6** on the basis of the solvatochromic analysis (see Table 3) and eq 2.[33]

$$\Delta\tilde{\nu}_{abs-em} = \Delta\tilde{\nu}^{vac}_{abs-em} + \frac{2(\mu_e - \mu_g)^2}{hc_0a_O^3}[f(\epsilon_r) - f(n^2)] \quad (2)$$

As shown in Table 2, the nonradiative rate constants change from ca. 4.5 to 1.5×10^8 s^{-1} upon going from nonpolar to polar solvents. These changes are considerably small, and the trends can be explained within the above-mentioned model. From studies of differently donor-substituted 4-(4′-donor-phenyl)terypyridines, it is known that such dyes with a weak donor in the 4′-phenyl position possess fluorescence lifetimes of ca. 1.2 ns and $k_{nr} \sim (4-5) \times 10^8$ s^{-1} in solvents of any polarity and their counterparts with a strong donor in the 4′-phenyl position show a behavior very similar to that of our title dyes; e.g., 4-[4′-(dimethylamino)phenyl]terpyridine shows $k_{nr} = 4.1 \times 10^8$ s^{-1} in cyclohexane and $k_{nr} = 1.4 \times 10^8$ s^{-1} in dichloromethane.[34]

In the weakly 4′-donor-substituted 4-phenylterpyridines as well as 2,4,6-triphenylpyridines, the emitting state is basically the (relaxed) Franck−Condon state with a weak ICT character. In the dyes with a strong 4′-donor, the presence of less polar solvents thus shifts the features of the ICT state back toward the former derivatives, i.e., toward the (relaxed) Franck−Condon state. Because monoexponential fluorescence decays on the picosecond time scale were always found, the Franck−Condon−ICT state dynamics, however, must occur on the subpicosecond time scale. The fact that the (relaxed) Franck−Condon state has a somewhat higher intrinsic nonradiative rate constant than the ICT state remains yet to be investigated with adequate methods and model compounds.

Having established the principle similarities of the photophysics of all four compounds, the subtle differences of the optical properties of the dyes as imposed by the variations of the substituents on the anilino group will be discussed. With respect to the parameters derived from the absorption and fluorescence features, molecules **1** and **5** always exhibit the extreme cases. **1** (**5**) shows the largest (smallest) Stokes shift in ACN, the largest (smallest) difference between the maxima in ACN and HEX, the lowest (highest) κ_f, the steepest (shallowest) slope of the solvatochromic plot, and the highest (lowest) change in the dipole moment ($\mu_e - \mu_g$). Thus, although being separated by ethylene groups from the anilino N atom, the other heteroatoms of the crown unit attached to the aniline apparently influence the electronic properties of the entire chromophore, most probably via a modulation of the redox potential or electron donor capacity of the anilino moiety. To gain better insight into these features, electrochemical studies of **1**, **2**, **5**, and **6** and some of their precursors were performed.

Electrochemical Measurements. The electrochemical behavior of compounds **I**, **II**, **V**, **VI**, **1**, **2**, **5**, and **6** were studied by cyclic voltammetry, rotating-disk electrochemistry, and differential pulse voltammetry. Linear sweep voltammetry showed for **I** an oxidation peak at 750 mV. When the two methyl groups of **I** are replaced by a macrocycle containing three O atoms, the oxidation wave shifts to 786 mV. For **V** and **VI**, the oxidation process is shifted to still higher potentials of ca. 820 mV. In all cases, when the sweep is reversed after the oxidation peak, the corresponding reduction peak is not detected or very poorly defined, indicating that the redox process is irreversible. A closely related behavior was observed for **1**, **2**, **5**, and **6**. In this case, the aniline moiety is irreversibly oxidized in the 800−900 mV region (Table 4). Moreover, the anilinopyridines show a reduction peak between ca. −2200 and −2300 mV (Table 4). For all of these compounds, when the sweep is reversed, the corresponding oxidation peak is observed. However, the differences between the cathodic and anodic peak potentials ($\Delta E_P > 150$ mV) and the ratio between the anodic andcathodic intensities (i_a/i_c ca. 0.5−0.7) are far from those expected for a reversible route, suggesting a quasi-reversible process. Figure 3 shows the differential pulse voltammograms recorded for compounds **1** and **5** in ACN. For the anilinopyridines, it is found that with increasing substitution,

(29) $f(\epsilon) - f(n^2)$ with $f(\epsilon) = (\epsilon - 1)/(2\epsilon + 1)$, $f(n^2) = (n^2 - 1)/(2n^2 + 1)$, and ϵ and n being the dielectric constant and the refractive index. See: Lippert, E. *Z. Naturforsch.* **1955**, *10a*, 541−545. Lippert, E. *Z. Elektrochem.* **1957**, *61*, 962−975. Mataga, N.; Kaifu, Y.; Koizumi, M. *Bull. Chem. Soc. Jpn.* **1956**, *29*, 465−470.

(30) The angle θ between the aniline and pyridine rings was determined as 21.5° in the X-ray analysis of **5** and is obtained as 38° ± 1° for all of the dyes in quantum chemical calculations employing the AM1 method with the AMPAC 6.55 package.

(31) Maus, M.; Rettig, W.; Bonafoux, D.; Lapouyade, R. *J. Phys. Chem. A* **1999**, *103*, 3388−3401.

(32) For the mathematical background of the vibrational analysis, see ref 31.

(33) $\Delta\tilde{\nu}^{vac}_{abs-em}$ is the extrapolated Stokes shift in a vacuum, μ_g and μ_e are the ground- and excited-state dipole moments, a_O is the Onsager cavity radius, ϵ is the relative permittivity of the respective solvent, and the other constants include speed of light in a vacuum (c_0) and Planck's constant (h). a_O (ca. 5.7 Å) and μ_g (3−4 D) were taken from the optimized geometries of **1**, **2**, **5**, and **6** as obtained by quantum chemical calculations.

(34) Goodall, W.; Wild, K.; Arm, K. J.; Williams, J. A. G. *J. Chem. Soc., Perkin Trans. 2* **2002**, 1669−1681.

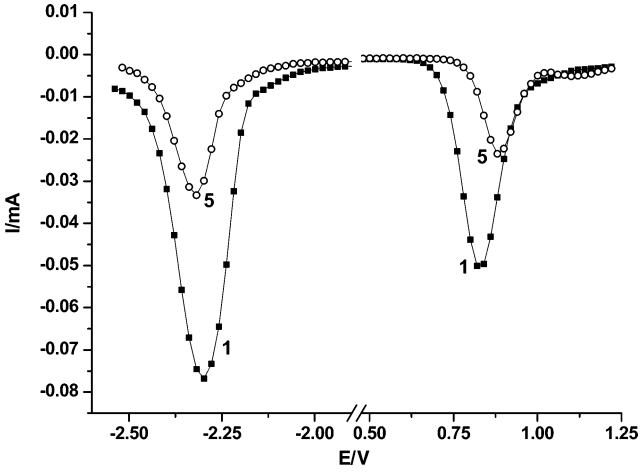

Figure 3. Differential pulse voltammetry of **1** and **5** in ACN (Pt working electrode; 0.1 M tetrabutylammonium perchlorate).

Table 4. Redox Potentials of **I**, **II**, **V**, **VI**, **1**, **2**, **5**, and **6** in ACN Measured vs SCE

	$E_{1/2}$(ox)[a]/mV	$E_{1/2}$(red)[a]/mV
I	750	
II	786	
V	826	
VI	816	
1	816	−2300
2	840	−2300
5	876	−2180
6	856	−2300

[a] Data from rotating-disk electrode experiments (0.1 M $NBu^n_4ClO_4$) in ACN (see the Experimental Section).

i.e., upon introduction of the crown units instead of the methyl groups, the oxidation potentials are shifted to more positive potentials,[35] suggesting that the cation is destabilized and the electron density in the molecule is lowered. This reduction in the donor strength proceeds from **1** via **2** and **6** to **5** (or, alternatively, from **I** via **II** and **VI** to **V**), reflecting well the findings on the subtle changes of the ICT character along the series as detailed in the previous section. Because of the fact that the substituents on the pyridine ring were kept constant in the title compounds, the reduction potentials were generally less affected.

Because we are interested in the structure−property relationships of such chromophoric systems to predict spectroscopic behavior, we correlated the electrochemical data with the results from quantum chemical calculations. Here, a plot of the calculated charge on the anilino N atom, Q_N, as derived by a procedure described in ref 36, vs the experimentally obtained $E_{1/2}$(ox) yields a linear relationship (Figure 4). Moreover, the complementarity of the spectroscopic, electrochemical, and theoretical data is further supported by the calculated highest occupied molecular orbital (HOMO)−lowest unoccupied molecular orbital (LUMO) gaps $\Delta E_{HOMO-LUMO}$ of 8.195 (for **1**), 8.103 (for **2**), 8.076 (for **6**), and 8.055 eV (for **5**), with the order reflecting again the experimental findings. In a continuation of our earlier works on the correlation of the theoretical and

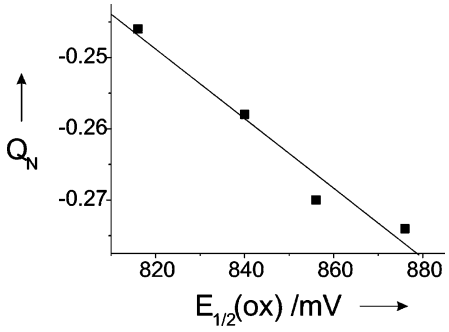

Figure 4. Plot of the charge on the anilino N atom, Q_N, of the optimized ground-state geometry vs the measured $E_{1/2}$(ox) for **1**, **2**, **5**, and **6**.

Table 5. pK_a Data and Spectroscopic Properties of the Mono- and Diprotonated Forms of **1**, **2**, **5**, and **6** in Ethanol−Water (50:50)

	pK_a(1)	pK_a(2)	ΔpK_a	λ_{abs}(C−H$^+$)/nm	λ_{abs}(C−2H$^+$)/nm
1	3.26 ± 0.02	0.83 ± 0.02	2.43	443	334
2	3.54 ± 0.05	1.29 ± 0.03	2.25	441	334
5	2.77 ± 0.01	−0.16 ± 0.01	2.93	430	335
6	3.23 ± 0.01	0.63 ± 0.02	2.60	438	336

experimental results of crowned chromo- and fluoroionophores,[36] the present studies suggest that rational tools will become increasingly important in the development of functional dyes and molecular probes.

Spectroscopic Protonation Studies. As discussed above, **1**−**6** possess two protic sites that contain a N atom as the donor and acceptor moieties of a conjugated π-electron system. The pK_a's of the parent compounds aniline and triphenylpyridine amount to 4.65[37] (in water) and 1.84[38] [in ethanol−water (70:30)], respectively. The question thus was, in what respect do the π conjugation of both units and the choice of secondary heteroatoms of the macrocycle modulate the protonation behavior, i.e., shifts the pK_a and reflects the findings of the structure−property relationships. pH titrations of **1**, **2**, **5**, and **6** were carried out in ethanol−water (50:50) mixtures, and the results are included in Table 5. In all of the cases, the two protonation steps are sufficiently separated by Δp$K > 2$ to allow reliable analysis of the single branches of the titration curve. Representative titration spectra and curve of **5** are shown in Figure 5.

The results reveal that for all of the dyes the addition of protons leads first to the development of a new and more intense band in the 430−440 nm region, a decrease of the band at 335 nm, and the shift of the second maximum to 320 nm, corresponding to a change of the solution from colorless to yellow (Figure 5). When higher acid concentrations are employed, the red-shifted band is again bleached and the neighboring, weaker band is shifted back from 320 to 335 nm. The initial batho- and hyperchromic shifts of the ICT band are conceivable with protonation of the pyridine unit, increasing its acceptor strength and leading to a decrease

(35) Mortimer, R. J.; Weightman, J. S. *J. Electroanal. Chem.* **1996**, *418*, 1−7.

(36) Rurack, K.; Sczepan, M.; Spieles, M.; Resch-Genger, U.; Rettig, W. *Chem. Phys. Lett.* **2000**, *320*, 87−94.

(37) *Critical Stability Constants*; Smith, R. M., Martell, A. E., Eds.; Plenum: New York, 1974; Vol. 2.

(38) Katritzky, A. R.; Leahy, D. E.; Maquestiau, A.; Flammang, R. *J. Chem. Soc., Perkin Trans. 2* **1983**, 45−48.

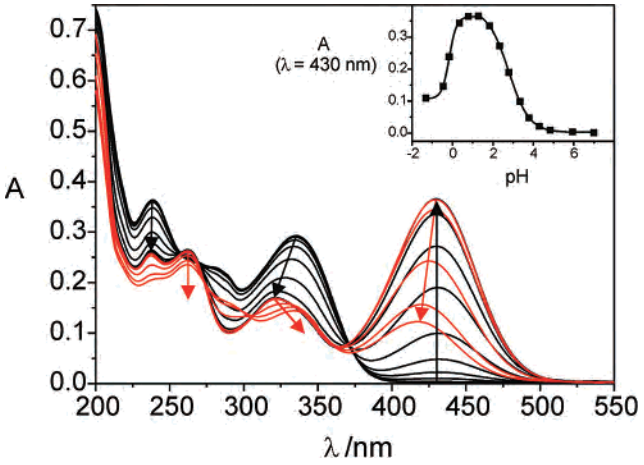

Figure 5. Absorption spectra of **5** as a function of the pH: 7.0 > pH > 1.3 in black and 1 > pH > −1.3 in red. The inset shows the absorption changes at 430 nm (symbols) and the fits of the two regions (black lines).

of the interannular twist angle.[39] The second proton then attacks the anilino N atom, reducing its donor strength and leading to the hypsochromic shift in strongly acidic media. This is additionally reflected in the decrease of the typical anilino-located transition at 265 nm in the acidic part of the titration. The $\Delta pK > 2$ and the presence of clear isosbestic points in all of the cases strongly suggest that protonation only takes place successively and that the order of basicity of the two subunits is reversed by their assembly in a π-conjugated chromophore. No correlation is found between the order of $pK_a(1)$ or $pK_a(2)$ and $E_{1/2}(ox)$ of **1**, **2**, and **6**. Only for **5** do the distinctly lower pK_a's seem to be a direct consequence of the redox features. For the other three dyes, the order of pK_a primarily depends on the size and type of the heteroatom in the macrocycle. For instance, a small crown with three additional O atoms that can support the protonation of the anilino N atom by hydrogen bonding leads to the distinctly higher $pK_a(2)$ of **2**. On the other hand, the presence of the two distant S atoms in **6** leads to a lower $pK_a(2)$ for **6** as compared to **1** with electronically rather neutral methyl substituents. In **5**, the two bulky S atoms in the direct neighborhood of the anilino N atom effectively shield the N atom and aggravate protonation. The effects described here for ethanol−water solutions are even more pronounced in ACN, where, for instance, **5** shows again a color change to yellow upon the addition of protons, but for **2**, the solution remains colorless and only the low-energy absorption band is shifted hypsochromically from 343 to 322 nm. The latter is consistent with preferential protonation of the aniline, presumably being strongly stabilized in the above-mentioned sense by hydrogen bonding in the small monoaza−trioxa macrocycle in the nonprotic solvent. This conclusion is supported by the spectroscopic properties of unsubstituted 2,4,6-triphenylpyridine, which shows absorption maxima at 315 nm in toluene and at 310 nm in ethanol.[40,41]

Fluorescence measurements of the dyes in the presence of protons support the UV/vis spectroscopic findings. Whenever protonation occurs at the pyridino acceptor site, excitation in the red-shifted absorption band gives rise to a red-shifted fluorescence band at 580 ± 3 nm in ACN. In accordance with reports on (dimethylanilino)alkylpyridinium[42] and (dimethylamino)pyrimidine[43] dyes, both the fluorescence quantum yield and the lifetime of the bathochromic bands are significantly reduced, e.g., showing Φ_f between 5×10^{-4} and 5×10^{-3} and $\tau_f \leq 30$ ps in the highly polar solvent. As put forth in ref 42, we tentatively attribute the fluorescence features of the acceptor protonated dyes with the rapid population of a highly twisted ICT state—twisted around the interannular bond—in contrast to the virtually planar emissive state in the unprotonated molecules, vide supra. In general, emission from such excited CT states with perpendicular conformation is largely forbidden, and in the case of the (dimethylanilino)alkylpyridinium dyes, accelerated internal conversion was assumed to contribute to the strongly reduced fluorescence yield.[42] The effects of protonation at the anilino side as found for **2**−H^+ are manifested in a hypsochromic shift of the fluorescence band to 363 nm, consistent with the decrease in the donor strength upon anilinium cation formation. Moreover, in the presence of a large excess of protons, where presumably species with both protonated donor and acceptor exist, this band shifts back to longer wavelengths, to 408 nm. Both values correspond well to the fluorescence behavior of the parent 2,4,6-triphenylpyridine:[40] emission of the neat dye (which lacks any donor in the 4 position) is centered at 351 nm, whereas protonation of the acceptor leads to a shift of the emission to 410 nm, reflecting the step from singly to doubly protonated **2**.

Spectroscopic Studies Involving Metal Cations. The behavior observed upon the addition of different cations to ACN solutions of **1**−**6** can be rationalized in a fashion similar to that described above for protonation processes. The ICT transition at ca. 340 nm would be shifted to ca. 440 nm when the cation coordinates with the pyridine group, strengthening its acceptor character. On the contrary, no band in the visible will be formed if coordination takes place solely at the aniline group. Additionally, if a metal ion coordinates to both sites with different affinities, shifted bands and the absence of clear isosbestic points would be expected. Complete studies of metal coordination were carried out with **1**, **2**, **5**, and **6**, yielding four different behaviors: selective coordination at the pyridine, selective coordination at the aniline, mixed coordination at both sites, and no coordination.

The addition of Cu^{2+}, Zn^{2+}, Hg^{2+}, Pb^{2+}, and Fe^{3+} to ACN solutions of **1** resulted in the development of the band at

(39) A reduction of θ from ca. 38° to ca. 25° is found by quantum chemical calculations.

(40) Kurfürst, A.; Lhotak, P.; Petru, M.; Kuthan, J. *Collect. Czech. Chem. Commun.* **1989**, *54*, 462−472. Druzhinin, S. I.; Dmitruk, S. L.; Lyapustina, S. A.; Uzhinov, B. M.; Makarova, N. I.; Knyazhanskii, M. I. *J. Photochem. Photobiol., A* **1992**, *68*, 319−335.

(41) The behavior of **3** and **4** is very similar to that of **1**, indicating that the small size of the crown in **2** is mandatory for the observed stabilization by hydrogen bonding.

(42) Ephardt, H.; Fromherz, P. *J. Phys. Chem.* **1991**, *95*, 6792−6797. Fromherz, P.; Heilemann, A. *J. Phys. Chem.* **1992**, *96*, 6864−6866. Röcker, C.; Heilemann, A.; Fromherz, P. *J. Phys. Chem.* **1996**, *100*, 12172−12177. Rettig, W.; Kharlanov, V.; Maus, M. *Chem. Phys. Lett.* **2000**, *318*, 173−180.

(43) Herbich, J.; Grabowski, Z. R.; Wójtowicz, H.; Golankiewicz, K. *J. Phys. Chem.* **1989**, *93*, 3439−3444.

437 nm, indicating a (at least partial) coordination of these cations to the electron-accepting pyridine unit. However, only for Zn^{2+} and Pb^{2+} are clear isosbestic points observed so that for Cu^{2+}, Hg^{2+}, and Fe^{3+} partial coordination at the anilino group also takes place. When the intensity of the 437 nm band of 5.0×10^{-5} M solutions of **1** is monitored during a titration with Zn^{2+} and Pb^{2+}, the complex stability constants log K for the formation of $[Zn(\mathbf{1})]^{2+}$ and $[Pb(\mathbf{1})]^{2+}$ were determined to 4.60 ± 0.20 and 4.39 ± 0.03, respectively, with nonlinear least-squares fits assuming a 1:1 ligand-to-metal stoichiometry yielding acceptable results.[44] ^{1}H NMR studies confirmed the above-described coordination behavior; i.e., only small shifts of 0.01, 0.03, and 0.15 ppm were found for the methylanilino signals upon the addition of 2 equiv of Zn^{2+} to **1** in CD_3CN. In contrast, the resonances corresponding to pyridine and the 2,6-phenyl rings were shifted by +0.12, −0.26, and +0.10 ppm, indicating preferential coordination at the pyridine.[45] Corresponding measurements with Hg^{2+} (2 equiv) yielded stronger shifts for the methyl (0.25 ppm) and anilino fragments (0.80 and 0.25 ppm) as compared to those for the pyridine (0.12 ppm) and the phenyl protons (−0.20 and +0.15 ppm), pointing to mixed coordination with a preference for the anilino site reflected by the absence of isosbestic points in the spectrophotometric titrations. Other transition-metal ions such as Ni^{2+} and Cd^{2+} were unable to coordinate and thus did not change the UV/vis spectra or ^{1}H NMR shifts of **1** at micromolar concentrations.

Similar to **1**, **2** forms well-defined 1:1 complexes of log $K = 4.29 \pm 0.07$ and 3.81 ± 0.09 with Zn^{2+} and Pb^{2+}, respectively, manifested in the appearance of a band at 445 nm, while Fe^{3+}, Cu^{2+}, and Hg^{2+} gave a more complicated titration pattern indicative of the formation of different metal−aniline and metal−pyridine coordination complexes. Again, the first-row metal cations Ni^{2+} and Cd^{2+} showed no interaction with **2**.

Interestingly, **5** behaves again very differently in the sense that the two S atoms close to the anilino N atom strongly shield this site against complexation with all non-thiophilic cations. It is known that this crown selectively coordinates Hg^{2+} over other transition-metal ions.[5e,13a,46] The presence of the dioxa−dithia−aza crown in **5** thus forces all of the cations except Hg^{2+} to be coordinated by the pyridine moiety. In contrast to **1** and **2**, Cu^{2+} and Fe^{3+} show a behavior for **5** similar to that of Zn^{2+} and Pb^{2+} and yield bathochromically (at 440 nm) absorbing 1:1 complexes with log K values of 4.60 ± 0.20 for $[Cu(\mathbf{5})]^{2+}$ and 6.6 ± 0.4 for $[Fe(\mathbf{5})]^{3+}$, while 4.86 ± 0.08 and 4.50 ± 0.20 are found for $[Pb(\mathbf{5})]^{2+}$ and $[Zn(\mathbf{5})]^{2+}$, respectively. In contrast, binding of Hg^{2+} to the crown engages the lone electron pair of the anilino N atom in coordination and leads to a reduction of the ICT character and a shift of the absorption band from 340 to 310 nm. The different responses of **1** and **5** toward Hg^{2+} are shown in Figure 6. Again for **5**, the addition of Ni^{2+} and Cd^{2+} does not induce a measurable change of the properties. The change in the position of the S atoms in the macrocyclic cavity between **5** and **6** does not induce significant variations, and only $[Hg(\mathbf{6})]^{2+}$ absorbs at 317 nm. The different responses of **5** and **6** toward protons and cations clearly reflect the importance of receptor topology. Cations with a coordination number of ≥6 are less sensitive to the arrangement of secondary heteroatoms in the crown than protons to the immediate neighborhood of their single designated binding site at the anilino N atom. In addition to these coordination features in ACN, **5** and **6** can also act as selective probes for the detection of Hg^{2+} in a mixed aqueous solution by complexing it with the crown ether unit.

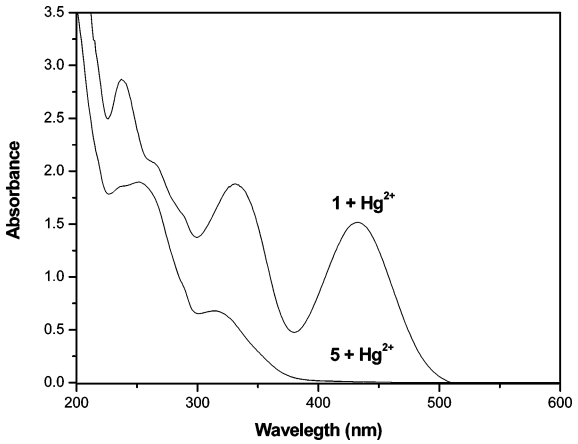

Figure 6. Different UV/vis responses of **1** and **5** ($c_{ligand} = 3 \times 10^{-5}$ M) toward Hg^{2+} ($c_{cation} = 3 \times 10^{-5}$ M) in ACN.

The behavior of **3** and **4** toward cations is again very similar to that of **1** and **2**. Colorless ACN solutions turned bright yellow upon the addition of equimolar quantities of Hg^{2+} and Cu^{2+}. However, the fact that the intensity of the band at 441 nm was rather low suggests that interaction with the anilino crown occurs, too, yet with a lower formation constant. The opposite effect is observed for Fe^{3+}, Pb^{2+}, and Zn^{2+}, where equimolar quantities induce only a pale-yellow color, revealing less preference for binding to the acceptor site. The lack of isosbestic points in titrations of **3** and **4** with Fe^{3+}, Pb^{2+}, and Zn^{2+} supports the findings of coordination at both sites with different formation constants. Cd^{2+} and Ni^{2+} are again spectroscopically silent.

Selected fluorescence studies of the compounds in the presence of cations that are representative of a certain spectroscopic behavior again support the photometric results and reinforce the mechanistic conclusions drawn. As in the case of protons, excitation in the red-shifted absorption band induced by cation coordination to the pyridino acceptor generates a red-shifted emission band, being centered between 550 and 580 nm as a function of the charge density and the coordinating ability of the cation. For instance, in the case of **5**, the cornerstones are $[Pb(\mathbf{5})]^{2+}$ with a maximum at 563 nm and $[Fe(\mathbf{5})]^{3+}$ with $\lambda_{em} = 582$ nm. Moreover, in general, the fluorescence of complexes with paramagnetic metal ions is even more strongly reduced than that of complexes with the d^{10} metal ions. Taking **5** as an example, representative fluorescence lifetimes amount to 31 ps for [Pb-

(44) Bourson, J.; Pouget, J.; Valeur, B. *J. Phys. Chem.* **1993**, *97*, 4552−4557.
(45) Note that Herbich et al. also found exclusive coordination of Zn^{2+} ions to the pyrimidino N atoms in (dimethylamino)pyrimidine dyes.[43]
(46) Ros-Lis, J. V.; Martínez-Máñez, R.; Rurack, K.; Sancenón, F.; Soto, J.; Spieles, M. *Inorg. Chem.* **2004**, *43*, 5183−5185.

(**5**)]$^{2+}$ and ca. 5 ps for [Fe(**5**)]$^{3+}$ in ACN (for the limiting instrumental resolution, see the Experimental Section). Following the interpretation of the effects of Zn^{2+} binding on the emission features of (dimethylamino)pyrimidines,[43] we assume also an analogy between the effects of protonation and metal binding. Thus, the red-shifted and strongly quenched fluorescence of the complexes should also involve the formation of an intramolecularly twisted CT excited state. The special case of exclusive coordination in the crown ether moieties of [Hg(**5**)]$^{2+}$ and [Hg(**6**)]$^{2+}$ is also reflected by the fluorescence properties of the complex. In contrast to the strong hypsochromic shift in absorption, the emission band of this complex is only moderately shifted to shorter wavelengths, to 421 nm. This behavior could be explained in terms of cation decoordination in the excited state: the coordinative bond between the ion and anilino N atom is weakened by the ICT process because of increasingly electrostatic repulsion between the positively charged cation and the reduced charge density at the donor. Similar observations have been made for a number of donor−acceptor-substituted fluoroionophores with a cation-responsive receptor in the donor part of the molecule.[26c,47] Interestingly, the Hg^{2+} complexes of **5** and **6** maintain their emission behavior in a mixed aqueous solution.

Anion Sensing through the Development of Differential Anion Chemosensing Ensembles. The UV/vis studies carried out with **1**−**6** showed that the coordination to the pyridine or aniline groups can be modulated by the different crown ether moieties attached to the anilino N atom. Following Scheme 1, we have now a tool in hand to pursue certain paths from panel II to III or from panel II to IV by choice of the appropriate combination of **DA** ditopic dye and cation. For instance, from panel II to III, a selective Hg^{2+} coordination to the substituted aniline framework is achieved when using an aza−oxa−thia crown as **D** (compound **5** in Scheme 2). Additionally, an anion-signaling mechanism can also be envisaged as sketched in Scheme 1. The CT absorption band of a certain chromophoric ligand **DA** can be modulated by particular cations **M** that coordinate to the pyridine acceptor part of the chromophore (**DA**−**M**). As a consequence, the strength of the acceptor is increased and the ICT band is shifted to longer wavelengths; the yellow color appears. Addition of an anion (**X**) to **DA**−**M** can then lead to the formation of ion pair−complex conjugates (**DA**−**M**−**X**), which might induce changes in the **DA**−**M** coordination, i.e., weakening of the ligand−metal ion bond or modifying the preferential coordination of the cation to the aniline or pyridine groups. The latter would result in a modulation of the absorption band. Bearing in mind the forces at play, the response of certain **DA**−**M** pairs toward a certain anion **X** would depend on the intrinsic chemical nature of the metal and anion such as valence, charge density, hard- and softness of both metal cations and anion, etc. These subtle differences should then be reflected in the specific spectral fingerprints of each **DA**−**M**−**X**. In the overall protocol, a combination of certain **DA** with different **M** can yield a family of differential signaling ensembles for the pattern recognition of anions.

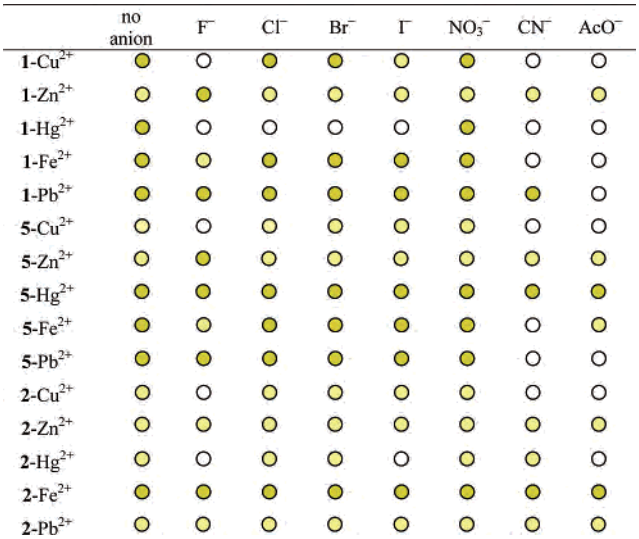

Figure 7. Schematic representation of the color variations of **1**−**M**, **5**−**M**, and **2**−**M** ensembles (**M** = Cu^{2+}, Zn^{2+}, Hg^{2+}, Fe^{3+}, and Pb^{2+}) in the presence of 1 equiv of anion. For clarity, the colors of the solutions have been classified as dark yellow (absorbance of 1 ± 0.2 for the band at 430 nm), pale yellow (absorbance of 0.5 ± 0.1), and colorless (absorbance of 0 ± 0.1). Except for Cl^-, Br^-, and NO_3^- anions, clear selectivity patterns in accordance with Scheme 1, panel IV, can be observed for the anions.

As a proof-of-principle, we have prepared a library of differential anion chemosensors from **1**, **2**, and **5** as ditopic ligands and cations Cu^{2+}, Zn^{2+}, Hg^{2+}, Fe^{3+}, and Pb^{2+}. These **DA**−**M** pairs constitute a wide range of different species, namely, (i) cation coordination to the functionalized aniline (**D**), (ii) cation coordination to the substituted pyridine (**A**), or (iii) a blending of species with mixed **A**/**D** coordination of the cation. Moreover, an important prerequisite of the protocol is that only metal salts with counteranions that have a distinctly weaker affinity to the cations than the target anions are used and that a nonprotic solvent showing a relatively weak coordination with cations is employed. The combinations of ditopic ligands and various cations are then assumed to show gradual and differential responses toward the target anions **X**, which all were monovalent in the present experiments. To test the ability of the ensembles, ACN solutions of the different **DA**−**M** pairs were prepared and mixed with aliquots of solutions containing 1 equiv of F^-, Cl^-, Br^-, I^-, NO_3^-, AcO^-, or CN^-. Depending on the preferential coordination of the cation and the strength of the **X**−**M** interaction, three different colorimetric responses were found: (i) partial or complete decoloration (indicating a weakening of the **A**−**M** bond by formation of the corresponding ionic pair **DA**−**M**−**X**), (ii) color enhancement (tentatively assigned to a partial anion-induced coordination rearrangement from **D**−**M** to **A**−**M**), and (iii) no effect. The response pattern has been summarized in Figure 7, with a color code denoting each general type of response. This is

(47) Martin, M. M.; Plaza, P.; Dai Hung, N.; Meyer, Y. H.; Bourson, J.; Valeur, B. *Chem. Phys. Lett.* **1993**, *202*, 425−430. Dumon, P.; Jonusauskas, G.; Dupuy, F.; Pée, P.; Rullière, C.; Létard, J.-F.; Lapouyade, R. *J. Phys. Chem.* **1994**, *98*, 10391−10396. Mathevet, R.; Jonusauskas, G.; Rullière, C.; Létard, J.-F.; Lapouyade, R. *J. Phys. Chem.* **1995**, *99*, 15709−15713. Martin, M. M.; Plaza, P.; Meyer, Y. H.; Badaoui, F.; Bourson, J.; Lefevre, J.-P.; Valeur, B. *J. Phys. Chem.* **1996**, *100*, 6879−6888.

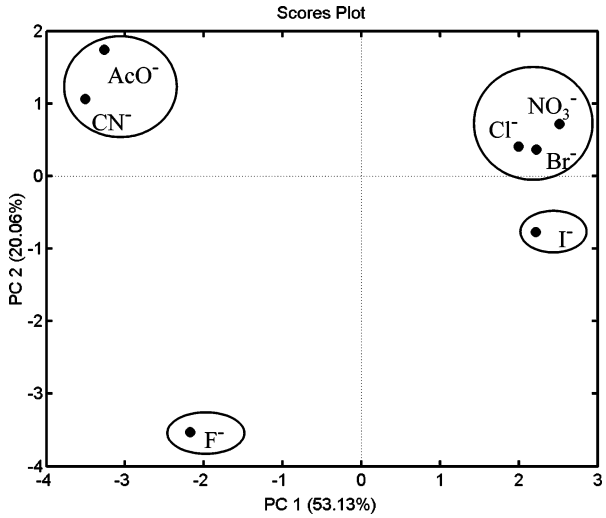

Figure 8. PCA score plot for different anions using a set of **DA**−**M** chromogenic probe complexes (**DA** = **1**, **2**, and **5**; M = Cu^{2+}, Zn^{2+}, Fe^{3+}, Hg^{2+}, and Pb^{2+}). Principal component axes are calculated to lie along lines of diminishing levels of variance in the data set.

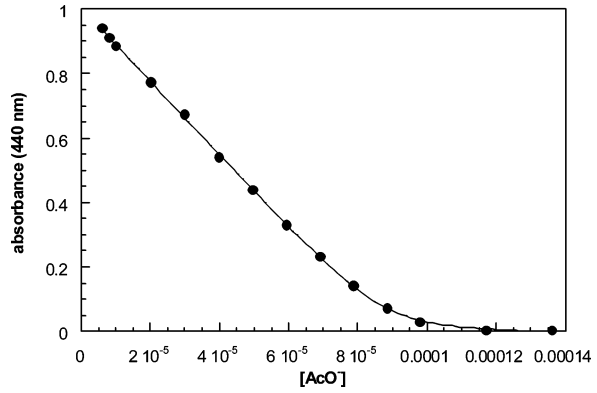

Figure 9. Variation of the intensity of the band at 440 nm for the ensemble **5**−**Pb** upon the addition of increasing amounts of acetate in ACN.

the experimental outcome of the designed chemosensing concept described above in Scheme 1, panel IV. From Figure 7, it is evident that except for NO_3^-, Cl^-, and Br^-, which gave a very similar response with all of the **DA**−**M** ensembles, clear selectivity "fingerprints" can be observed for the other anions when the entire matrix is analyzed by algorithms such as principal component analysis (PCA).[48] Figure 8 shows the PCA plot for the data in Figure 7. Recognition patterns could be identified for AcO^-, CN^-, I^-, and F^-, whereas the proximity between scores for Cl^-, Br^-, and NO_3^- indicates a too high similarity in color variation with the present **DA**−**M**'s. It is also remarkable that in some cases even a truly selective chromogenic response, e.g., for **5**−**Pb** and acetate and for **5**−**Fe** and cyanide.

As we have reported in a preliminary communication,[14] fluorescence lifetime studies were carried out to elucidate the reason of the decoloration processes upon anion addition, i.e., whether it is due to simple dissociation of the complex or to the formation of a ternary conjugate. The studies were carried out with the **5**−**Pb**−**X** system and revealed that indeed a ternary conjugate is formed where **Pb** and **X** seem to be ion-paired and **Pb** and **5** are still bound by a weak coordinative bond. Additionally, titrations of **5**−**Pb** with acetate and benzoate indicated the formation of 1:1 adducts (Figure 9). For instance, log K was determined to 6.40 ± 0.30 for the formation of **1**−**Pb**−**AcO** by nonlinear least-squares fitting. In fact, it is also remarkable that the system is quite robust and tolerates up to 2 vol % of water without significant changes with respect to its behavior. Thus, for instance, we have previously demonstrated that the **5**−**Pb** system can be used for the colorimetric determination of acetic acid in a vinegar using ACN−water mixtures (98:2 vol %).[14]

Conclusion

A family of ditopic chromoionophores **DA** containing two coordination sites, a monodentate 2,6-diphenylpyridine acceptor (**A**) moiety, and an anilino donor (**D**) group with different macrocyclic receptors has been prepared and characterized, and their prospective use for cation and anion signaling has been studied. Investigation of the optical and electrochemical properties of the molecules revealed that the donor (**D**) and acceptor (**A**) groups are strongly π-conjugated, entailing intense ICT absorption bands at ca. 340 nm. Coordination studies with protons and cations showed that a shift of the ICT band from 340 nm to the visible (ca. 440 nm) occurs upon coordination at the pyridine group. On the other hand, only a hypsochromically shifted band is formed if a proton or cation binds to the aniline. For various members of the family, a rich metal coordination behavior was found modulated by the nature of the ring denticity and types of secondary heteroatoms in the macrocycle. A certain selective coordination was found, for instance, using **5** and Hg^{2+}, which can be used for the detection of this cation in a mixed aqueous solution. Finally, the **M**−**DA** ensembles were prospectively used as an array of differential receptors for chromogenic anion (**X**) sensing via the formation of an ion pair−complex conjugate (**DA**−**M**−**X**) and modulations of the **M**−**A** or **M**−**D** coordination preferences. Various patterns of spectral changes were obtained, and analysis of the data yielded clear differential recognition patterns for acetate, fluoride, iodide, and cyanide anions. These studies demonstrate that it might be possible to prepare simple chromogenic host−guest pairs that show gradual responses toward a third type of chemical species, e.g., anions. Because the strategy introduced here takes profit of coordination chemistry using relatively weak coordinating and nonhydrating solvents while tolerating a sufficient amount of water to allow for the analysis of realistic samples,[14] the common disadvantage of many chromogenic probes being non-water-soluble is turned into a key feature of the present protocol. In such a way, we have demonstrated that relatively undemanding chromogenic molecular systems that are facile to prepare can be employed for unspecific but differential recognition in the sense described in panel IV of Scheme 1.

(48) Jolliffe, I. T. *Principal Component Analysis*; Springer: New York, 2002.

Acknowledgment. We thank the Ministerio de Ciencia y Tecnología (Project CTQ2006-15456-C04-01) and Universidad Politécnica de Valencia for support. F.S. thanks the Ministerio de Educación y Ciencia for a Ramón y Cajal contract.

Supporting Information Available: X-ray crystallographic data in CIF format. This material is available free of charge via the Internet at http://pubs.acs.org.

IC062069Z